

## Resonance-enhanced high-order harmonic generation by combination of an infrared laser field and a time-delayed attosecond XUV pulse

Yun-He Xing , Jun Zhang, Mei-Lian He, Xiao-Xin Huo, Shuang Wang, Zi-An Li, and Xue-Shen Liu\*  
*Institute of Atomic and Molecular Physics, Jilin University, Changchun 130012, China*

 (Received 20 April 2024; revised 26 July 2024; accepted 13 August 2024; published 30 August 2024)

We investigate theoretically the high-order harmonic generation of the molecular ion  $H_3^{2+}$  by numerically solving the two-dimensional time-dependent Schrödinger equation. The results show that a resonant harmonic with large ellipticity is generated and the harmonic efficiency is significantly enhanced when the infrared laser field is combined with a time-delayed attosecond extreme-ultraviolet (XUV) laser pulse. The generation of resonant harmonics can be understood as the electron transition between the ground and excited states through the absorption of XUV photons. By varying the time delay and amplitudes of the two laser pulses, we can obtain the harmonics close to circular polarization in the resonant region. The input XUV pulse is linearly polarized, while the generated resonant harmonics are elliptically polarized, which means that the input XUV pulse can be reshaped. Moreover, we investigate the dependence of the resonant harmonic on the laser polarization, which shows the sensitivity of the harmonic polarization to the laser polarization and the resonance state can also be changed by changing the direction of polarization of the laser field.

DOI: [10.1103/PhysRevA.110.023118](https://doi.org/10.1103/PhysRevA.110.023118)

### I. INTRODUCTION

The high-order harmonic generation (HHG) by the interaction between an intense laser field and atoms or molecules is a highly nonlinear phenomenon. The physical process of HHG can be clearly described by a three-step model [1]. HHG is an ideal source for generating attosecond-pulse, soft x-ray, and extreme-ultraviolet (XUV) light [2–4]. XUV light has proven to be a very important and powerful tool for controlling the electronic dynamics of atoms and molecules [5].

The resonance enhancement effects of HHG are of particular interest; these effects can be exploited to improve harmonic conversion efficiencies [6–8]. Therefore, the generation of resonance-enhanced below-threshold harmonics has been extensively investigated [9–11]. However, the polarization characteristic of below-threshold harmonics has been less investigated. For a long time, harmonics were limited to linear polarization. Elliptically polarized (EP) or even circularly polarized (CP) radiation in the XUV and soft x-ray spectral regions is of great importance in applications, especially in the areas of chiral recognition of molecules [12], magnetic circular dichroism spectroscopy [13,14], and probe-spin dynamics [15].

The simplest scheme to obtain CP harmonics is from a CP driving-laser field. But the harmonic efficiency decreases significantly with increasing the ellipticity of the driving-laser field [16,17]. Moreover, the EP harmonics can be obtained by designing various forms of the two-dimensional driving fields, for example, cross-linearly polarized two-color laser fields [18,19] and combined laser fields [20–22]. On the other hand, EP harmonics can also be obtained by preparing specific target

molecules or atoms [23–25]. However, this method generates relatively small ellipticity. In addition, improving the conversion efficiency of harmonics is also a key point. Ishikawa [26,27] found that the harmonic intensity from  $He^+$  was significantly enhanced by the combination of the ultrashort intense fundamental laser and its high-order harmonic pulses. Harmonic enhancement can be understood as the laser field driving a superposition state between the  $1s$  and  $2s$  states from  $He^+$ . The driving-laser field used in this scheme is a linearly polarized laser field and acts on an isotropic medium. Therefore, the radiation harmonics are linearly polarized. Moreover, the emission efficiency of high-order harmonics can also be enhanced by the resonance effect of HHG [28–30]. These research works have shown that the resonance effect of HHG can effectively enhance the intensity of the harmonics, but little attention has been paid to the polarization properties of these resonance harmonics.

In order to obtain high-intensity XUV radiation with large ellipticity, the single-electron molecular ion  $H_3^{2+}$  is used as a benchmark model for understanding strong-field molecular ionization dynamics. The equilateral-triangular molecular ion  $H_3^{2+}$  is a complex geometry that provides a richer feature of HHG than atoms. Due to its unique geometry, it provides a fundamentally original system for the theoretical development of the nonperturbative response of nonlinear molecules to intense laser pulses. Using  $H_3^{2+}$  as a research target to study the process of HHG has been reported [31–34].

In this paper, we investigate the resonance-enhanced high-order harmonic of the molecular ion  $H_3^{2+}$  by an infrared (IR) laser field combined with an attosecond XUV laser pulse through the numerical solution of the two-dimensional time-dependent Schrödinger equation. By varying the time delay of the two laser pulses, a below-threshold harmonic with large ellipticity can be generated in the resonance region. The input

\*Contact author: liuxs@jlu.edu.cn

IR and XUV pulses are linearly polarized, while the generated resonance harmonics are elliptically polarized. This means that the input XUV pulse can be reshaped. We illustrate the dependence of the resonant harmonic intensity and ellipticity on the driving-laser strength. Moreover, we investigate the dependence of the resonance harmonics on the laser polarization, which shows the influence of the molecular geometry on the resonance harmonics and the resonant state is also sensitive to the direction of polarization of the laser pulses.

## II. THEORETICAL METHODS

To investigate the HHG and electron dynamics in an intense laser field, we numerically solve the two-dimensional time-dependent Schrödinger equation (2D TDSE) in the length gauge (atomic units are used unless otherwise stated),

$$i \frac{\partial}{\partial t} \psi(x, y, t) = H(x, y, t) \psi(x, y, t), \quad (1)$$

where  $H(x, y, t) = -\frac{1}{2} \nabla_{x,y}^2 + V_C(x, y) + V_I(x, y, t)$  is the full Hamiltonian.  $V_C(x, y)$  is the Coulomb potential of the molecular ion  $H_3^{2+}$ , which is given by

$$V_C(x, y) = \sum_{i=1}^3 -\frac{1}{\sqrt{(x - N_{ix})^2 + (y - N_{iy})^2 + a}}, \quad (2)$$

where the nuclear coordinates  $N_{ix}$  and  $N_{iy}$  are fixed by the relations  $N_{1x} = 0$ ,  $N_{2x} = -R \sin(\theta/2)$ ,  $N_{3x} = R \sin(\theta/2)$ ,  $N_{1y} = (2/3)R \cos(\theta/2)$ ,  $N_{2y} = -(1/3)R \cos(\theta/2)$ , and  $N_{3y} = -(1/3)R \cos(\theta/2)$ .  $R = 2$  a.u. is the equilibrium internuclear distance, and  $\theta = 60^\circ$  is the angle between the two molecular bonds. The geometry of the molecular ion  $H_3^{2+}$  in the  $(x, y)$  plane is shown in Fig. 1(a).  $a = 0.35$  a.u. is the soft-core parameter, which is used to eliminate the Coulomb singularity and obtain the energy of certain electronic states in the molecular ion  $H_3^{2+}$  [31,35].  $V_I(x, y, t) = xE_x(t) + yE_y(t)$  represents the interaction between the molecule and the laser fields. The total external field is along the  $x$ -axis direction [ $E_y(t) = 0$ ], which is expressed as

$$E(t) = E_x(t) = E_1 f_1(t) \cos(\omega_1 t) \hat{e}_x + E_2 f_2(t - \Delta\tau) \cos[\omega_2(t - \Delta\tau)] \hat{e}_x, \quad (3)$$

where  $f_1(t) = \sin^2[\pi t/T_1]$  and  $f_2(t - \Delta\tau) = e^{-2 \ln(2)[(t - \Delta\tau)/T_2]^2}$  are the envelopes of the IR and XUV laser pulses, respectively.  $T_1 = 8T$  [ $T = 2\pi/\omega_1$  is an optical cycle (o.c.) of the IR laser field] is the pulse duration of the IR laser field.  $T_2 = 600$  as is the FWHM of the XUV laser pulse.  $E_1$  ( $\omega_1$ ) and  $E_2$  ( $\omega_2$ ) are the amplitudes (frequencies) of the IR and XUV laser fields, respectively.  $\Delta\tau$  is the time delay of the XUV pulse with respect to the IR laser field.

The 2D TDSE is solved by using the second-order splitting-operator fast-Fourier-transform algorithm [36]. We use a grid of size 409.6 a.u. containing 2048 grid points on the  $x$  ( $y$ ) axis. The space and time steps are 0.4 and 0.05 a.u., respectively. To prevent unphysical reflection of the electron wave packet from the boundary, the wave function is multiplied by a  $\cos^{1/8}$  “mask function” at each time step [37]. The time-dependent dipole acceleration in the  $x$  and  $y$  directions

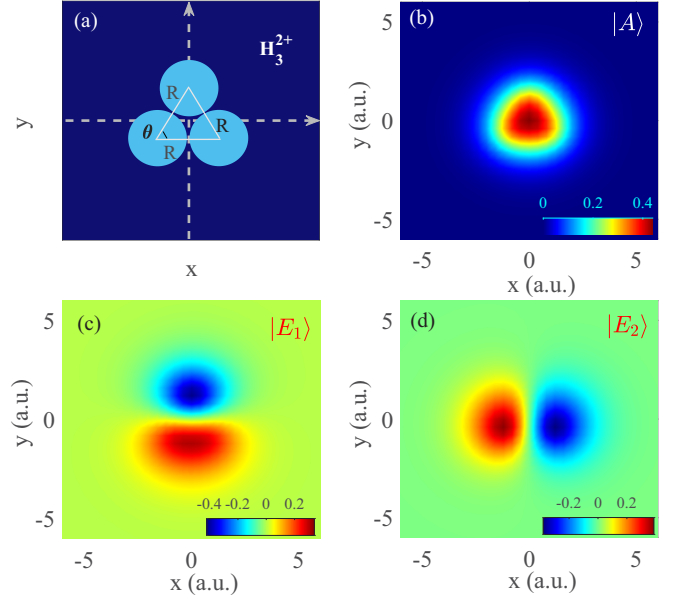


FIG. 1. (a) Illustration of the molecular system  $H_3^{2+}$  with equilateral-triangle geometry.  $R$  denotes the molecular internuclear distance, and  $\theta$  is the bond angle between the two bonds of the molecule. (b) The wave function of the ground  $|A\rangle$  state. (c) and (d) The degenerate excited  $|E_1\rangle$  and  $|E_2\rangle$  states, respectively, which are obtained with the imaginary-time-evolution method.

can be obtained using Ehrenfest’s theorem:

$$d_x(t) = \langle \psi(x, y, t) | -\frac{\partial V_C(x, y)}{\partial x} - E_x(t) | \psi(x, y, t) \rangle \hat{e}_x, \\ d_y(t) = \langle \psi(x, y, t) | -\frac{\partial V_C(x, y)}{\partial y} - E_y(t) | \psi(x, y, t) \rangle \hat{e}_y. \quad (4)$$

The corresponding HHG is proportional to the square modulus of the Fourier transformation of the dipole acceleration expectation value:

$$G_x(\omega) = \left| \frac{1}{T_f - t_0} \int_{t_0}^{T_f} d_x(t) e^{-i\omega t} dt \right|^2, \\ G_y(\omega) = \left| \frac{1}{T_f - t_0} \int_{t_0}^{T_f} d_y(t) e^{-i\omega t} dt \right|^2, \quad (5)$$

where  $t_0$  is the initial moment and  $T_f$  is the final moment. The ellipticity of the harmonics, as used in Ref. [38], can be expressed as

$$\varepsilon = \sqrt{\frac{1 + r^2 - \sqrt{1 + r^4 + 2r^2 \cos 2\delta}}{1 + r^2 + \sqrt{1 + r^4 + 2r^2 \cos 2\delta}}}. \quad (6)$$

$r = |a_y(\omega)|/|a_x(\omega)|$  and  $\delta = \varphi_y(\omega) - \varphi_x(\omega)$  are the amplitude ratio and phase difference of the  $y$  and  $x$  components of the harmonics, where  $a_{x,y}(\omega) = \int_{-\infty}^{\infty} d_{x,y}(t) e^{-i\omega t} dt$  and  $\varphi_{x,y}(\omega) = \arg[a_{x,y}(\omega)]$  [39]. To obtain a harmonic with large ellipticity, the amplitude ratio  $r$  and phase difference  $\delta$  need to be close to 1 and  $\pm\pi/2$ , respectively [40,41].

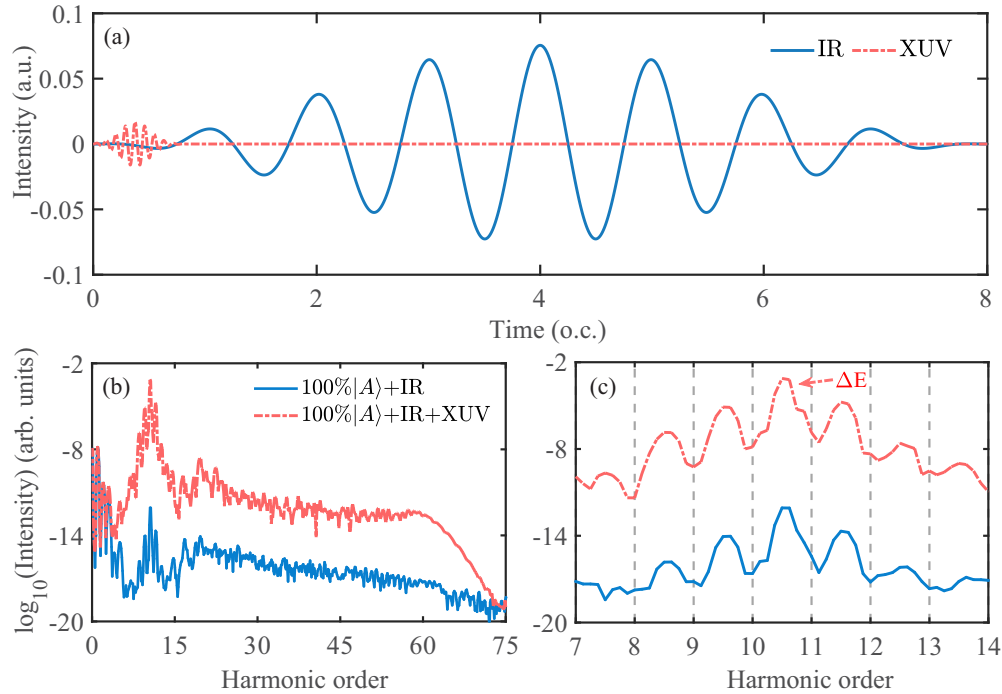


FIG. 2. (a) Electric fields of the IR (blue solid line) and attosecond XUV (red dashed line) laser pulses. The time delay of the XUV pulse with respect to the IR field is  $\Delta\tau = 0.375$  o.c. (b) The harmonic spectra of  $\text{H}_3^{2+}$  generated by the IR laser pulse alone (blue solid line) and the combined laser pulses (red dashed line) with time delay  $\Delta\tau = 0.375$  o.c. The initial states are prepared as the ground state. (c) Enlarged harmonic spectra from (b) corresponding to the 7th to 14th orders.

### III. RESULTS AND DISCUSSION

In this paper we focus on the generation of below-threshold harmonics through the resonance enhancement effect in HHG and investigate the physical mechanisms of harmonic enhancement as well as the polarization properties of the resonant harmonics.

In Fig. 1(a), we present the geometry of the molecular ion  $\text{H}_3^{2+}$  in the  $(x, y)$  plane. It is shown that  $\text{H}_3^{2+}$  is a triangular molecule with an equivalent internuclear distance. Figure 1(b) shows the wave function of the ground  $|A\rangle$  state with ionization energy  $I_{p_0} = 1.8$  a.u. (48.98 eV), as demonstrated in Ref. [31], which is obtained using the imaginary-time-evolution method. Figures 1(c) and 1(d) show the wave function of  $|E_1\rangle$  and  $|E_2\rangle$  states, which are orthogonal to each other. The  $|E_1\rangle$  and  $|E_2\rangle$  states are doubly degenerate with the same ionization energy,  $I_{p_1} = I_{p_2} = 1.2$  a.u. (32.65 eV) [31,42].

Figure 2(a) shows the electric fields of the IR laser field (blue solid line) and the attosecond XUV laser pulse (red dashed line). The wavelengths of the IR and XUV laser fields are  $\lambda_1 = 800$  nm ( $\omega_1 = 0.057$  a.u.) and  $\lambda_2 = 69$  nm ( $\omega_2 = 0.66$  a.u.), respectively. The peak strengths of IR and XUV laser pulses are  $2 \times 10^{14}$  and  $1 \times 10^{13}$  W/cm<sup>2</sup>, respectively. The time delay of the XUV pulse with respect to the IR pulse is  $\Delta\tau = 0.375$  o.c. The polarization of the IR field and the XUV pulse is along the  $x$  direction. FWHM of the XUV pulse is 600 attosecond with a Gaussian envelope, and the pulse duration of the IR pulse is 8 o.c. with a sin-square envelope. Figure 2(b) shows the harmonics spectrum for the molecular ion  $\text{H}_3^{2+}$  initially in the ground  $|A\rangle$  state exposed to only the

IR laser pulse ( $100\%|A\rangle + \text{IR}$ , indicated by the blue solid line) and the IR laser pulse combined with an attosecond XUV pulse ( $100\%|A\rangle + \text{IR} + \text{XUV}$ , indicated by the red dashed line) with time delay  $\Delta\tau = 0.375$  o.c.

We find that the harmonic intensity generated from the IR laser field alone is low, while the harmonic intensity is significantly enhanced when the XUV field is added. The intensities in the resonant and plateau regions are increased by about 9 and 5 orders of magnitude, respectively. Figure 2(c) shows the details of the resonant harmonics in Fig. 2(b) from the 7th to 14th order. From Fig. 2(c), we can see that all the harmonics generated in the resonance region (from 7th to 14th order) are half-integer harmonics, where peaks H10.5 and H11.5 have higher intensities. The generation of the strongest-resonance peak, H10.5, can be understood as follows. The resonant energy gap between the ground  $|A\rangle$  state and the excited  $|E_{1,2}\rangle$  states is  $\Delta E = I_{p_0} - I_{p_{1,2}} = 0.6$  a.u. (16.32 eV), which is close to the energy of H10.5 (16.29 eV). From Fig. 1(c), we can see that the  $|E_1\rangle$  state has a large electron density distribution in the  $y$  direction, while the  $|E_2\rangle$  state has a large electron density distribution in the  $x$  direction, as shown in Fig. 1(d). Due to the fact that the polarization directions of the IR field and the XUV pulse are both along the  $x$  direction, the motion of the electrons from the ground  $|A\rangle$  state tends to be along the polarization direction of the laser. Thus, the resonance transition from the ground  $|A\rangle$  state to the  $|E_2\rangle$  state will occur by absorbing an XUV photon  $\omega_2 = 0.66$  a.u. (17.95 eV), which is close to the energy gap  $\Delta E$  (16.32 eV). Thus, the generation of H10.5 can be understood as a result of the one-XUV-photon resonance transition.

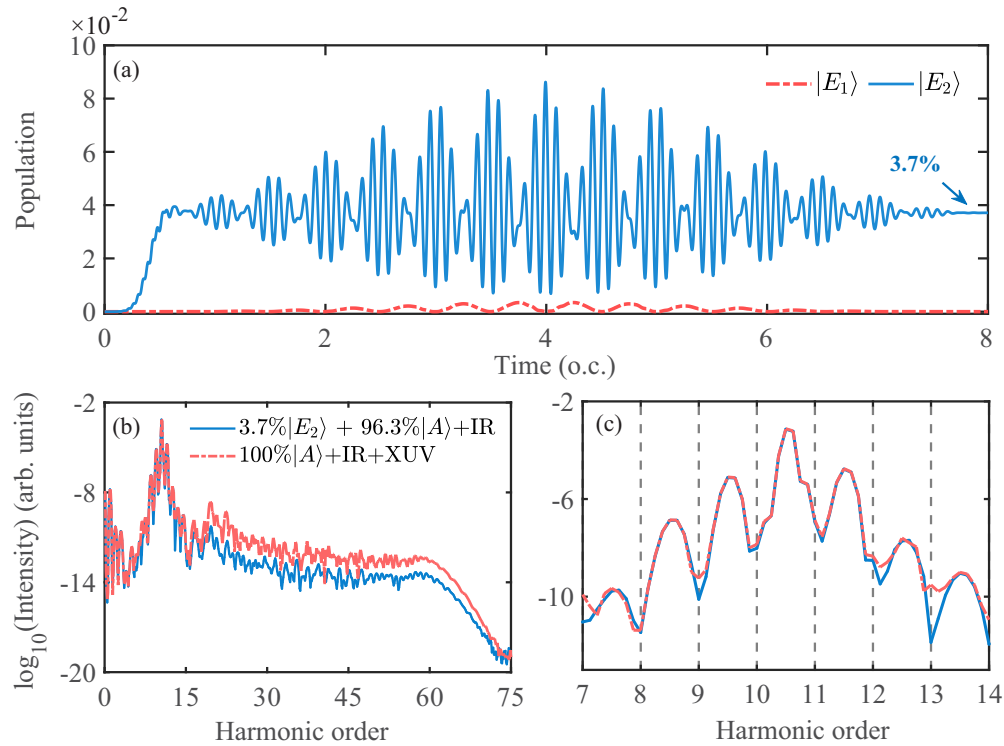


FIG. 3. (a) Populations on the  $|E_1\rangle$  (red dashed line) and  $|E_2\rangle$  (blue solid line) states of the molecular ion  $\text{H}_3^{2+}$  driven by the combined laser pulses with time delay  $\Delta\tau = 0.375$  o.c. (b) Harmonic spectrum (blue solid line) from a coherent superposition of the ground  $|A\rangle$  state (96.3%) and excited  $|E_2\rangle$  state (3.7%) exposed to the IR laser pulse alone and the harmonic spectrum (red dashed line) from the ground  $|A\rangle$  state (100%) exposed to the IR field combined with the XUV pulse with time delay  $\Delta\tau = 0.375$  o.c. (c) The harmonic spectra corresponding to (b), ranging from the 7th to 14th orders. The other laser parameters are the same as those in Fig. 1.

H10.5 and H11.5 are below-threshold harmonics dominated by multiphoton processes. Therefore, the generation of half-integer-order resonance peaks can be explained as a result of the multiphoton resonance. The main effect of the XUV pulse is a quick transfer of the population from the  $|A\rangle$  to  $|E_2\rangle$  state, which is similar to the effect of the short XUV pulse discussed in Ref. [43]. Tudorovskaya and Lein [43] illustrated that a long XUV pulse will induce Rabi oscillations in a two-level system, causing a Rabi splitting of the emission peaks (see Fig. 4 in Ref. [43]), which is similar to the Autler-Townes effect [44,45] in absorption lines and photoelectron spectra. In contrast, a short XUV pulse does not cause Rabi oscillations in the excited state, and the main effect of the short XUV pulse is to rapidly transfer the electron population from the ground state to the excited state, so the splitting of the resonance peaks will not be observed when the short XUV pulse is added to the IR field.

The  $|A\rangle$  state will be rapidly lifted to the  $|E_2\rangle$  state after absorbing an XUV photon, and this process also generates a superposition state ( $|A\rangle$  and  $|E_2\rangle$ ) [26,27]. Subsequently, the superposition state will be excited in the IR field. This process can be understood as follows: under an IR+XUV pulse, at first, the ground state is transferred to the  $|E_2\rangle$  state by absorbing an XUV photon ( $\omega_2$ ), producing a superposition state; then the superposition state is excited by absorbing an IR photon ( $\omega_1$ ) through the IR field, and finally, the energy (corresponding to H11.5 ( $\Delta E + \omega_1$ ) [43]) is generated.

It is worth noting that the physical mechanisms for the generation of below-threshold harmonics (H10.5, H11.5) and above-threshold harmonics are quite different. For example, after the generation of a superposition state by XUV pulse excitation, the enhancement of H11.5 originates from the fact that the electron in the superposition state absorbs an IR photon and then returns to the  $|A\rangle$  state (the electron is not ionized), which is easier than absorbing IR photons from the  $|A\rangle$  state to produce H11.5.

However, the enhancement of the above-threshold harmonics originates from the optical-field electron ionization of the electrons in the superposition state driven by the IR laser field. Since the  $|E_2\rangle$ -state level is only 1.2 a.u. (32.65 eV), which is below the ionization threshold, the electron can now be more easily lifted to the continuum than that in the  $|A\rangle$  state [1.8 a.u. (48.98 eV)] and, subsequently, can emit a harmonic photon upon recombination. This is similar to the three-energy-level system which was described in Refs. [26,46]. Here, we focus only on the resonant harmonics (H10.5 and H11.5).

To illustrate the mechanism of the resonant harmonic enhancement, we present the populations of the excited  $|E_1\rangle$  and  $|E_2\rangle$  states driven by the combined laser pulses (the IR laser field combined with the XUV pulse) with time delay  $\Delta\tau = 0.375$  o.c., as shown in Fig. 3(a). From Fig. 3(a) we can see that the population of the  $|E_2\rangle$  state increases rapidly from 0 to 0.5 o.c., followed by strong oscillations; about 3.7% of the electron population is left in the  $|E_2\rangle$  state at

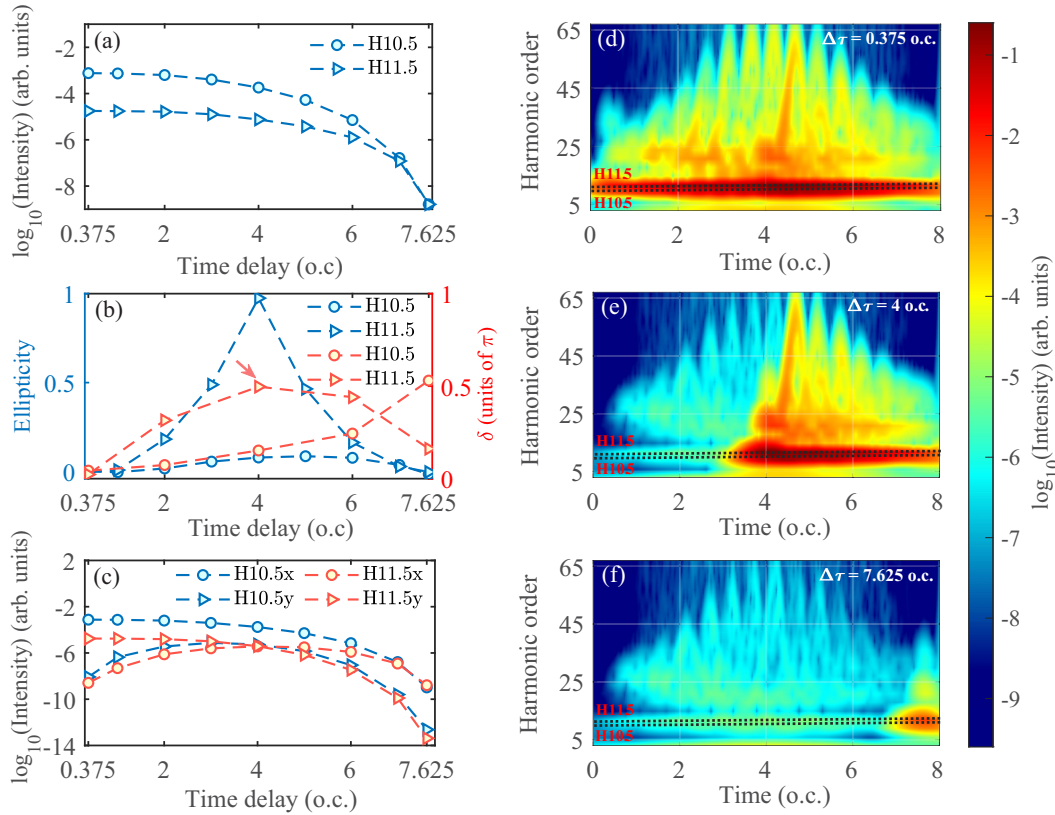


FIG. 4. (a) Intensity of the resonant harmonics (H10.5 and H11.5) for different  $\Delta\tau$ . (b) Ellipticity and phase difference  $\delta$  of the  $x$  and  $y$  components for the resonant harmonics (H10.5 and H11.5) with different  $\Delta\tau$ . (c) Intensity of the  $x$  and  $y$  components of the resonant harmonics (H10.5 and H11.5) for different  $\Delta\tau$ . The time-frequency distributions of the harmonic spectrum for different  $\Delta\tau$  at (d)  $\Delta\tau = 0.375$  o.c., (e)  $\Delta\tau = 4$  o.c., and (f)  $\Delta\tau = 7.625$  o.c.

the end of the laser pulses. However, the  $|E_1\rangle$  state is hardly excited, and the electron population is almost zero during the whole laser pulse. The above results indicate that the electrons are mainly excited to the  $|E_2\rangle$  state by absorbing an XUV photon, which triggers a resonance transition between the  $|A\rangle$  state and  $|E_2\rangle$  state. It is consistent with the analysis of the physical mechanism of H10.5 generation shown in Fig. 2(c). The results also show that only the  $|E_2\rangle$  state is related to the resonance enhancement process. Thus, this can be seen as a three-level system (ground, excited, and continuum states), as discussed in Refs. [26,46]. For our system, although there are two degenerate excited states ( $|E_1\rangle$ ,  $|E_2\rangle$ ), the population of the  $|E_1\rangle$  state is small, so it can also be understood as a three-level system ( $|A\rangle$ ,  $|E_2\rangle$ , and continuous states).

The resonance transition results in a superposition state, which is formed by the ground  $|A\rangle$  state with 96.3% of the electronic population and the excited  $|E_2\rangle$  state with 3.7% of the electronic population [27]. Figure 3(b) shows the harmonic spectrum from the superposition of the  $|E_2\rangle$  state (3.7%) and  $|A\rangle$  state (96.3%) exposed to the IR field alone and the harmonic spectrum from the ground  $|A\rangle$  state (100%) exposed to the combined laser pulses. Figure 3(c) shows the harmonic spectrum for the resonant harmonics from the 7th to 14th order, corresponding to Fig. 3(b). We can see that the position and intensity of the H11.5 resonance peak for the IR-driven superposition state and the IR+XUV-driven  $|A\rangle$

state match very well, which demonstrates the above analysis of the generation of H11.5.

In Fig. 4, we show the effect of the time delay of the IR and XUV pulse on the intensity and ellipticity for the two strongest resonance harmonics (H10.5, H11.5). We can see that the intensities of H10.5 and H11.5 decrease with the increase of the time delay, slower from  $\Delta\tau = 0.375$  o.c. to  $\Delta\tau = 4$  o.c. and faster from  $\Delta\tau = 4$  o.c. to  $\Delta\tau = 7.625$  o.c.

To understand the effect of resonant harmonics (H10.5, H11.5) with the time delay, we present the time-frequency analysis of the harmonics with  $\Delta\tau = 0.375$  o.c.,  $\Delta\tau = 4$  o.c., and  $\Delta\tau = 7.625$  o.c. in Figs. 4(d)–4(f), respectively.

From Fig. 4(a), we can see that the intensities of H10.5 and H11.5 are maximum when  $\Delta\tau = 0.375$  o.c. This can be attributed to the fact that the XUV pulse will generate a superposition state of  $|A\rangle$  and  $|E_2\rangle$ , and then the transition between the  $|A\rangle$  state and the  $|E_2\rangle$  state lasts for about 8 o.c., which results in the intensity of the H10.5 and H11.5 harmonics being strongest in this case. From Fig. 4(d), we can also see that the electron is mainly contributed to H10.5 and H11.5 during whole optical cycles (from 0 to 8 o.c.) with  $\Delta\tau = 0.375$  o.c. Thus, the intensities of H10.5 and H11.5 are strongest with  $\Delta\tau = 0.375$  o.c., as shown in Fig. 4(a).

The intensities of H10.5 and H11.5 decrease gradually with the increase of the time delay. This is due to the decrease in the duration of the superposition state generated by the transition between the  $|A\rangle$  and  $|E_2\rangle$  states in the XUV pulse. Therefore,

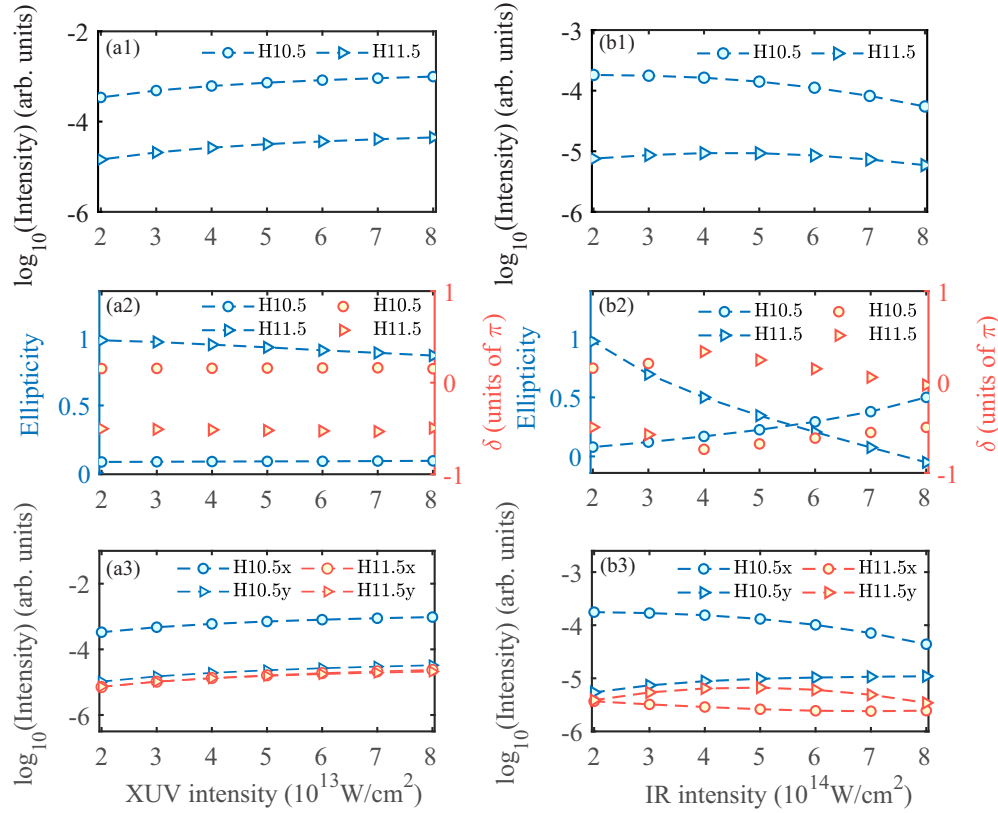


FIG. 5. (a1) Intensity, (a2) ellipticity and phase difference  $\delta$  of the  $x$  and  $y$  components, and (a3) intensity of the  $x$  and  $y$  components of the resonant harmonics (H10.5 and H11.5) for different peak strengths of XUV combined with a fixed IR field ( $I_1 = 2 \times 10^{14}$  W/cm<sup>2</sup>) at  $\Delta\tau = 4$  o.c. (b1) Intensity, (b2) ellipticity and phase difference  $\delta$  of the  $x$  and  $y$  components, (b3) intensity of the  $x$  and  $y$  components of the resonant harmonics (H10.5 and H11.5) for different peak strengths of IR combined with a fixed XUV pulse ( $I_2 = 1 \times 10^{13}$  W/cm<sup>2</sup>) at  $\Delta\tau = 4$  o.c. The other laser parameters are the same as in Fig. 1.

the intensities of H10.5 and H11.5 gradually decrease. From Fig. 4(e), we can see that, at  $\Delta\tau = 4$  o.c., the contributions of H10.5 and H11.5 are mainly from about 4 to 8 o.c., which agrees with the analysis above. For  $\Delta\tau = 7.625$  o.c., the harmonic intensities of H10.5 and H11.5 are very low, as shown in Fig. 4(a). From Fig. 4(f), we can see that the contribution to H10.5 and H11.5 is mainly from 7 to 8 o.c. Only a few electrons contribute to the resonance harmonics, which leads to a very low intensity.

Figures 4(b) and 4(c) show the ellipticity and the phase difference of the  $x$  and  $y$  components and the intensity of the  $x$  and  $y$  components for H10.5 and H11.5 when the time delay is increased from  $\Delta\tau = 0.375$  o.c. to  $\Delta\tau = 7.625$  o.c. From Fig. 4(b), we can see that the ellipticity of H11.5 increases and then decreases when the time delay is increased from  $\Delta\tau = 0.375$  o.c. to  $\Delta\tau = 7.625$  o.c. and has a maximum ellipticity of about  $\varepsilon = 1$  at  $\Delta\tau = 4$  o.c., which means that H11.5 is close to circularly polarized. The input XUV pulse is linearly polarized, while the generated H11.5 is close to circularly polarized with a large ellipticity. This indicates that the input XUV pulse can be reshaped. We know that the generation of harmonics with large ellipticity needs to meet two conditions. One of them is that the intensities of the  $x$  and  $y$  components of the harmonics must be comparable, and the other is that the phase difference of the  $x$  and  $y$  components of the harmonics must be close to  $\pm 0.5\pi$  [38,40,47]. From

Fig. 4(b) we can see that the phase difference of the  $x$  and  $y$  components of H11.5 is close to  $0.5\pi$  (red arrows) for  $\Delta\tau = 4$  o.c., and the intensities of the  $x$  and  $y$  components of H11.5 are comparable, as shown in Fig. 4(c) for  $\Delta\tau = 4$  o.c. Therefore, H11.5 has a large ellipticity for  $\Delta\tau = 4$  o.c. However, the ellipticity (blue line with circles) of H10.5 is close to zero when the time delay is increased from  $\Delta\tau = 0.375$  o.c. to  $\Delta\tau = 7.625$  o.c., as shown in Fig. 4(b). The phase difference of the  $x$  and  $y$  components of H10.5 is close to zero for  $\Delta\tau = 4$  o.c. [see red line with circles in Fig. 4(b)], and the intensities of the  $x$  and  $y$  components of H10.5 differ greatly [see Fig. 4(c), blue lines with circles and triangles]; thus, it does not satisfy the conditions for generating large ellipticity. The above results show that with an adjustment of the time delay of the IR and XUV pulses, the resonance harmonic (H11.5) has a large ellipticity with  $\Delta\tau = 4$  o.c..

To illustrate the dependence of H10.5 and H11.5 on the peak strength of the IR and XUV laser pulses, Fig. 5 presents the effect of the different peak strengths of IR and XUV on the ellipticity and intensity of H10.5 and H11.5 with  $\Delta\tau = 4$  o.c. Figure 5(a1) shows the intensity of H10.5 and H11.5 with different peak strengths (from  $2 \times 10^{13}$  to  $8 \times 10^{13}$  W/cm<sup>2</sup>) of the XUV pulse combined with a fixed IR laser field ( $2 \times 10^{14}$  W/cm<sup>2</sup>) with  $\Delta\tau = 4$  o.c. We find that the intensities of H10.5 and H11.5 increase proportionally with the increasing of the peak strength of the XUV pulse, which indicates that

the increase of the XUV strength will enhance the absorption of the XUV photon ( $\omega_2$ ) and lead to the enhancement of H10.5 ( $\Delta E$ ) and H11.5 [ $H10.5(\Delta E) + \omega_1$ ] [26]. From Fig. 5(a) we can see that, as the peak strength of the XUV pulse increases, the ellipticity of H10.5 is close to 0.1, and the ellipticity of H11.5 is very large (close to 1). And we can see that the phase differences of the  $x$  and  $y$  components of H10.5 and H11.5 are close to zero (red circles) and  $-0.5\pi$  (red triangles), respectively. From Fig. 5(a3), we find that the intensities of the  $x$  and  $y$  components of H10.5 are 1.6 orders of magnitude different, while they are equal for H11.5. Thus, the ellipticity of the H11.5 harmonic is large, and the ellipticity of H10.5 is small.

In Fig. 5(b1), we show the intensities of H10.5 and H11.5 with different IR field strengths (from  $2 \times 10^{14}$  to  $8 \times 10^{14}$  W/cm<sup>2</sup>) combined with the fixed XUV pulse strength ( $1 \times 10^{13}$  W/cm<sup>2</sup>) for  $\Delta\tau = 4$  o.c. From Fig. 5(b1), we can see that the intensities of H10.5 and H11.5 decrease gradually with the increase of the intensity of the IR field ( $>4 \times 10^{14}$  W/cm<sup>2</sup>), which can be attributed to the laser-induced Stark effect. From Fig. 5(b2) we find that the ellipticity of H10.5 increases from 0.17 to 0.5 and that of H11.5 decreases from 1 to 0 as the IR strength increases. The phase difference  $\delta$  of the  $x$  and  $y$  components of H10.5 gradually gets close to  $-0.5\pi$  (red circle), and the intensity difference of the  $x$  and  $y$  components of H10.5 gradually decreases as the IR strength increases [see blue lines with circles and triangles in Fig. 5(b3)], while the phase difference  $\delta$  of the  $x$  and  $y$  components of H11.5 is close to zero [see red triangles in Fig. 5(b2)], and the intensity difference of the  $x$  and  $y$  components of H11.5 gradually increases from  $2 \times 10^{14}$  to  $5 \times 10^{14}$  W/cm<sup>2</sup> and then decreases from  $5 \times 10^{14}$  to  $8 \times 10^{14}$  W/cm<sup>2</sup> [see red lines with circles and triangles in Fig. 5(b3)]. By analyzing the phase difference and the intensity of the  $x$  and  $y$  components of H10.5 and H11.5, we see the results are consistent with the variation of the ellipticity of the resonance harmonics (H10.5, H11.5). In order to explain the decrease in the intensities of the H10.5 and H11.5 with the increase in the intensity of the IR laser field ( $>4 \times 10^{14}$  W/cm<sup>2</sup>), Fig. 6(a) shows the distribution of harmonic intensity varies with the harmonic order and the intensity of the IR laser field. Figure 6(b) shows the intensities of H10.5 and H11.5 and the population of the  $|E_2\rangle$  state vary with the intensity of the IR field. In Ref. [48], the author indicated that the Stark effect will cause the energy levels to shift when the laser field is strong (see Fig. 7 of Ref. [48]). For weakly bound states such as Rydberg and continuous states, the Stark effect leads to an energy-level shift of approximately  $U_p$ , while the lower-order bound state is closer to the nucleus and has a smaller energy-level shift, as discussed in Ref. [48]. In Refs. [26,27], Ishikawa demonstrated that the laser-induced Stark effect will cause the expansion of the  $2p$  level of He<sup>+</sup> when the intensity of the fundamental laser field is greater than  $3 \times 10^{14}$  W/cm<sup>2</sup>. Thus, after the electron in the  $1s$  state absorbs an H27 photon, which corresponds to a full excitation of the  $1s - 2p$  state, the electron will transit to a virtual state which is close to the  $2p$  state. Thus, the resonance effect is weakened, and the intensity of the harmonic will decrease.

In our result, the intensities of H10.5 and H11.5 decrease as the intensity of the IR field increases when the intensity of the IR field is higher than  $4 \times 10^{14}$  W/cm<sup>2</sup>. The  $|E_2\rangle$  state

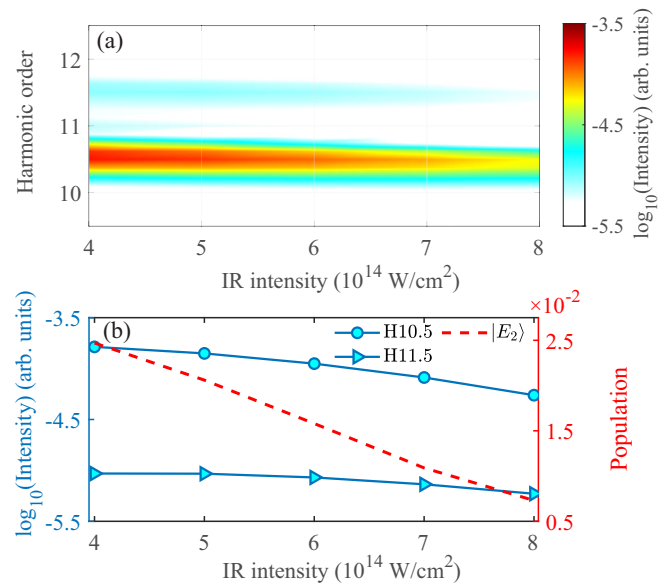


FIG. 6. (a) The distribution of harmonic intensity varying with the harmonic order and the intensity of the IR laser field. (b) The intensity of H10.5 and H11.5 and the population of the  $|E_2\rangle$  state varying with the intensity of the IR laser field. The other laser parameters are the same as those in Fig. 5(b1).

is a low-order bound state, and when the intensity of the IR field is enhanced, the  $|E_2\rangle$  energy level will shift very little, so the positions of the peaks (H10.5, H11.5) do not obviously shift [see Fig. 6(a)]. From Fig. 6(b), we can see that the population of the  $|E_2\rangle$  state gradually decrease, which is due to the energy-level shift caused by the laser-induced Stark effect. The electron in the  $|A\rangle$  state will transit to the virtual state which is close to the  $|E_2\rangle$  state by absorbing an XUV photon. Therefore, the resonance effect is weakened, and the intensities of H10.5 and H11.5 will be reduced. These results are consistent with our analysis above and with those discussed in Refs. [26,27].

In Fig. 7, we present the dependence of the intensity, the ellipticity of the resonant harmonics (H10.5, H11.5), and the population of the degenerate  $|E_1\rangle$  and  $|E_2\rangle$  states on the laser polarization with time delay  $\Delta\tau = 4$  o.c. The angle represents the angle between the polarization of the IR field and the XUV pulse with respect to the  $x$  axis. Figures 7(a) and 7(b) show the intensities and ellipticities of H10.5 and H11.5 when the laser polarization is increased from  $0^\circ$  to  $180^\circ$ . From Figs. 7(a) and 7(b) we can see that the intensities and ellipticities of H10.5 and H11.5 are symmetrically distributed about  $90^\circ$ , and as the angle increases from  $0^\circ$  to  $90^\circ$ , the intensity of H10.5 decreases and then increases, and the intensity of H11.5 remains constant, which can be attributed to the equilateral-triangular structure of  $H_3^{2+}$ . When the angle is increased from  $0^\circ$  to  $90^\circ$ , the polarization of the laser changes from parallel to one bond axis of  $H_3^{2+}$  to perpendicular to one bond axis. And when the angle is increased from  $90^\circ$  to  $180^\circ$ , the laser polarization changes from perpendicular to one bond axis of  $H_3^{2+}$  to parallel to one bond axis. In these two cases the response of the electrons to the laser pulse is the same; thus, the intensities and ellipticities of H10.5 and H11.5 are symmetrically distributed

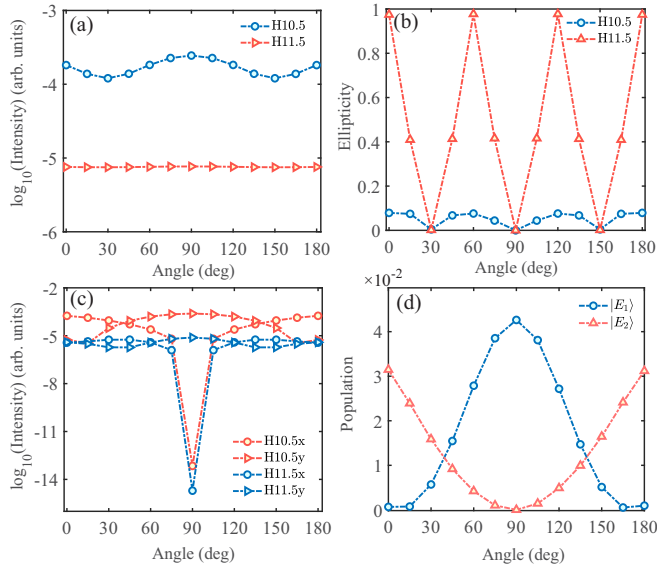


FIG. 7. (a) Intensity and (b) ellipticity of H10.5 and H11.5 for different laser polarization angles. (c) Intensity of the  $x$  and  $y$  components of H10.5 and H11.5 for different laser polarization angles. (d) Populations of the  $|E_1\rangle$  and  $|E_2\rangle$  states for different laser polarization angles. The time delay between IR and XUV is  $\Delta\tau = 4$  o.c. The other laser parameters are the same as those in Fig. 1.

about  $90^\circ$ . Moreover, from Fig. 7(b), we find that the ellipticities of H10.5 and H11.5 are zero for  $30^\circ$ ,  $90^\circ$ , and  $150^\circ$ . When the angles are  $30^\circ$ ,  $90^\circ$ , and  $150^\circ$ , the laser polarization is perpendicular to one of the bond axes of  $\text{H}_3^{2+}$ . In these cases, the wave function perpendicular to the laser polarization is symmetric. Take  $90^\circ$  as an example; the wave function satisfies  $\psi(x, y, t) = \psi(-x, y, t)$ . Therefore, the dipole moment in the  $x$  direction (perpendicular to the laser polarization) is zero according to  $\langle x \rangle = \int dy \int dx |\psi(x, y, t)|^2 x = 0$ . There is no harmonic generation in the  $x$  direction (the condition to generate large ellipticity is not satisfied, i.e., the intensities of the  $x$  and  $y$  components should be comparable), which is consistent with the intensities of the  $x$  direction of H10.5 and H11.5 for  $90^\circ$ , as shown in Fig. 7(c). From Fig. 7(a), we can see that the intensity of the H10.5 harmonic first decreases and

then increases in the ranges of  $0^\circ$  to  $90^\circ$  and  $90^\circ$  to  $180^\circ$ . The illustration in Fig. 2(c) shows that H10.5 is generated due to the electron transition between the ground  $|A\rangle$  state and the excited  $|E_2\rangle$  state (laser-pulse polarization along the  $x$  direction). The change in the polarization of the IR and XUV pulses will lead to a change in the resonance state. For example, at  $90^\circ$  the polarizations of IR and XUV are along the  $y$  direction, the electron motion is usually along the polarization of the laser pulse, and the wave function of the  $|E_1\rangle$  state is denser in the  $y$  direction [see Fig. 1(c)]. Therefore, the generation of H10.5 is due to the electron transition between the ground  $|A\rangle$  state and the  $|E_1\rangle$  state for  $90^\circ$ .

In Fig. 7(d), we can see that the population of the  $|E_1\rangle$  state is about 4%, while the population of the  $|E_2\rangle$  state is about 0% for  $90^\circ$ , which indicates that at  $90^\circ$  the generation of H10.5 originates from the electron transition between the ground  $|A\rangle$  state and the  $|E_1\rangle$  state. This is consistent with the analysis of the physical mechanism of H10.5 generation for  $90^\circ$ .

#### IV. CONCLUSIONS

In summary, we investigated theoretically the resonant harmonics from the molecular ion  $\text{H}_3^{2+}$  using an IR laser field combined with an XUV pulse. We found that the efficiency of the harmonics is significantly enhanced when the IR field is combined with an XUV pulse. Our results demonstrate that the physical mechanism of resonant harmonic generation can be understood as electronic transitions between the ground and excited states. By varying the time delay of the two lasers, we obtained EP harmonics in the resonance region. This means that we could reshape the input XUV pulse; i.e., the input pulse is linearly polarized, and the output pulse is elliptically polarized. The changes in laser polarization also caused the variation of resonance states. Moreover, when changing the peak strengths of the IR field and XUV pulse, the resonant harmonics with high ellipticity can still be obtained for a range of peak strengths. The ellipticity of the resonant harmonics is sensitive to the direction of laser polarization.

#### ACKNOWLEDGMENTS

This work was supported by the National Natural Science Foundation of China (Grants No. 12074142 and No. 12374265).

- [1] P. B. Corkum, *Phys. Rev. Lett.* **71**, 1994 (1993).
- [2] X. Zhang, X. Zhu, X. Liu, D. Wang, Q. Zhang, P. Lan, and P. Lu, *Opt. Lett.* **42**, 1027 (2017).
- [3] J. Li, X. Ren, Y. Yin, K. Zhao, A. Chew, Y. Cheng, E. Cunningham, Y. Wang, S. Hu, Y. Wu, M. Chini, and Z. Chang, *Nat. Commun.* **8**, 186 (2017).
- [4] J. Henkel, T. Witting, D. Fabris, M. Lein, P. L. Knight, J. W. G. Tisch, and J. P. Marangos, *Phys. Rev. A* **87**, 043818 (2013).
- [5] F. Krausz and M. Ivanov, *Rev. Mod. Phys.* **81**, 163 (2009).
- [6] Y. H. Lai, K. S. Rao, J. Liang, X. Wang, C. Guo, W. Yu, and W. Li, *Opt. Lett.* **46**, 2372 (2021).
- [7] M. A. Fareed, V. V. Strelkov, N. Thiré, S. Mondal, B. E. Schmidt, F. Légaré, and T. Ozaki, *Nat. Commun.* **8**, 16061 (2017).
- [8] M. A. Khokhlova, M. Y. Emelin, M. Y. Ryabikin, and V. V. Strelkov, *Phys. Rev. A* **103**, 043114 (2021).
- [9] K. N. Avanaki, D. A. Telnov, and S.-I. Chu, *Phys. Rev. A* **90**, 033425 (2014).
- [10] S. Beaulieu, S. Camp, D. Descamps, A. Comby, V. Wanie, S. Petit, F. Légaré, K. J. Schafer, M. B. Gaarde, F. Catoire, and Y. Mairesse, *Phys. Rev. Lett.* **117**, 203001 (2016).
- [11] W.-H. Xiong, J.-W. Geng, J.-Y. Tang, L.-Y. Peng, and Q. Gong, *Phys. Rev. Lett.* **112**, 233001 (2014).
- [12] R. Cireasa, A. E. Boguslavskiy, B. Pons, M. C. H. Wong, D. Descamps, S. Petit, H. Ruf, N. Thiré, A. Ferré, J. Suarez, J. Higuett, B. E. Schmidt, A. F. Alharbi, F. Légaré, V. Blanchet, B. Fabre, S. Patchkovskii, O. Smirnova, Y. Mairesse, and V. R. Bhardwaj, *Nat. Phys.* **11**, 654 (2015).

- [13] O. Kfir, P. Grychtol, E. Turgut, R. Knut, D. Zusin, D. Popmintchev, T. Popmintchev, H. Nembach, J. M. Shaw, A. Fleischer, H. Kapteyn, M. Murnane, and O. Cohen, *Nat. Photon.* **9**, 99 (2015).
- [14] D. D. Hickstein, F. J. Dollar, P. Grychtol, J. L. Ellis, R. Knut, C. Hernández-García, D. Zusin, C. Gentry, J. M. Shaw, T. Fan, K. M. Dorney, A. Becker, A. Jaroń-Becker, H. C. Kapteyn, M. M. Murnane, and C. G. Durfee, *Nat. Photon.* **9**, 743 (2015).
- [15] F. Willems, C. T. L. Smeenk, N. Zhavoronkov, O. Kornilov, I. Radu, M. Schmidbauer, M. Hanke, C. von Korff Schmising, M. J. J. Vrakking, and S. Eisebitt, *Phys. Rev. B* **92**, 220405(R) (2015).
- [16] P. Dietrich, N. H. Burnett, M. Ivanov, and P. B. Corkum, *Phys. Rev. A* **50**, R3585 (1994).
- [17] N. H. Burnett, C. Kan, and P. B. Corkum, *Phys. Rev. A* **51**, R3418 (1995).
- [18] Y. Fang and Y. Liu, *Phys. Rev. A* **103**, 033116 (2021).
- [19] D. Habibović, W. Becker, and D. B. Milošević, *Phys. Rev. A* **106**, 023119 (2022).
- [20] K.-J. Yuan and A. D. Bandrauk, *Phys. Rev. A* **83**, 063422 (2011).
- [21] N. Sun, X. Zhu, B. Wang, D. Wang, R. Shao, P. Lan, and P. Lu, *Phys. Rev. A* **101**, 053437 (2020).
- [22] R. Shao, C. Zhai, Y. Zhang, N. Sun, W. Cao, P. Lan, and P. Lu, *Opt. Express* **28**, 15874 (2020).
- [23] T. Kanai, S. Minemoto, and H. Sakai, *Phys. Rev. Lett.* **98**, 053002 (2007).
- [24] J. Levesque, Y. Mairesse, N. Dudovich, H. Pépin, J.-C. Kieffer, P. B. Corkum, and D. M. Villeneuve, *Phys. Rev. Lett.* **99**, 243001 (2007).
- [25] X. Zhou, R. Lock, N. Wagner, W. Li, H. C. Kapteyn, and M. M. Murnane, *Phys. Rev. Lett.* **102**, 073902 (2009).
- [26] K. Ishikawa, *Phys. Rev. Lett.* **91**, 043002 (2003).
- [27] K. L. Ishikawa, *Phys. Rev. A* **70**, 013412 (2004).
- [28] V. V. Strelkov, *Phys. Rev. A* **94**, 063420 (2016).
- [29] B. Wang, L. He, F. Wang, H. Yuan, X. Zhu, P. Lan, and P. Lu, *Opt. Express* **25**, 17777 (2017).
- [30] P.-C. Li, Z.-B. Wang, and S.-I. Chu, *Phys. Rev. A* **103**, 043113 (2021).
- [31] K. J. Yuan, S. Chelkowski, and A. D. Bandrauk, *J. Phys. Chem. A* **125**, 7111 (2021).
- [32] K.-J. Yuan, C. Lefebvre, S. Chelkowski, H. Lu, and A. D. Bandrauk, *Phys. Rev. A* **101**, 023411 (2020).
- [33] C. Lefebvre, H. Z. Lu, S. Chelkowski, and A. D. Bandrauk, *Phys. Rev. A* **89**, 023403 (2014).
- [34] A. D. Bandrauk, F. Mauger, and K.-J. Yuan, *J. Phys. B* **49**, 23LT01 (2016).
- [35] D. S. Tchitchekova, H. Lu, S. Chelkowski, and A. D. Bandrauk, *J. Phys. B* **44**, 065601 (2011).
- [36] M. D Feit, J. Fleck, Jr., and A. Steiger, *J. Comput. Phys.* **47**, 412 (1982).
- [37] X.-L. Ge, H. Du, J. Guo, and X.-S. Liu, *Opt. Express* **23**, 8837 (2015).
- [38] S.-K. Son, D. A. Telnov, and S.-I. Chu, *Phys. Rev. A* **82**, 043829 (2010).
- [39] F. Dong, Y. Tian, S. Yu, S. Wang, S. Yang, and Y. Chen, *Opt. Express* **23**, 18106 (2015).
- [40] X.-X. Huo, Y.-H. Xing, T. Qi, Y. Sun, B. Li, J. Zhang, and X.-S. Liu, *Phys. Rev. A* **103**, 053116 (2021).
- [41] H. Du, L. Luo, X. Wang, and B. Hu, *Phys. Rev. A* **86**, 013846 (2012).
- [42] A. D. Bandrauk and J. Ruel, *Phys. Rev. A* **59**, 2153 (1999).
- [43] M. Tudorovskaya and M. Lein, *J. Mod. Opt.* **61**, 845 (2014).
- [44] B. Tóth, A. Tóth, and A. Csehi, *J. Phys. B* **57**, 055002 (2024).
- [45] K. N. Avanaki, D. A. Telnov, and S.-I. Chu, *Phys. Rev. A* **94**, 053410 (2016).
- [46] J. B. Watson, A. Sanpera, X. Chen, and K. Burnett, *Phys. Rev. A* **53**, R1962 (1996).
- [47] J. Heslar, D. A. Telnov, and S.-I. Chu, *Phys. Rev. A* **96**, 063404 (2017).
- [48] M. Protopapas, C. H. Keitel, and P. L. Knight, *Rep. Prog. Phys.* **60**, 389 (1997).